Experimental study on low temperature desalination by flash evaporation in a novel compact chamber design

Jana Stengler [a], Karlheinz Schaber [b], Susanne Mall-Gleissle [c] *

[a] Institute of Engineering Thermodynamics, German Aerospace Center (DLR)
Pfaffenwaldring 38-40, 70569 Stuttgart, Germany
[b] Institute of Technical Thermodynamics and Refrigeration, Karlsruhe Institute of Technology (KIT)
Engler-Bunte-Ring 21, 76131 Karlsruhe, Germany
[c] Department of Mechanical and Process Engineering, Offenburg University of Applied Sciences
Badstraße 24, 77652 Offenburg, Germany

*Corresponding Author. Tel.: +49 781 205-4790. Email address: susanne.mall-gleissle@hs-offenburg.de

1 Abstract

The production of potable water in dry areas nowadays is mainly done by the desalination of seawater. State of the art desalination plants usually are built with high production capacities and consume a lot of electrical energy or energy from primary resources such as oil. This causes difficulties in rural areas, where no infrastructure is available neither for the plants' energy supply nor the distribution of the produced potable water. To address this need, small, self-sustaining and locally operated desalination plants came into the focus of research. In this work, a novel flash evaporator design is proposed which can be driven either by solar power or by low temperature waste heat. It offers low operation costs as well as easy maintenance. The results of an experimental setup operated with water at a feed flow rate of up to 1,600 l/h are presented. It is shown that the proof of concept regarding efficient evaporation as well as efficient gas-liquid separation is provided successfully. The experimental evaporation yield counts for 98 % of the vapor content that is expected from the vapor pressure curve of water. Neither measurements of the electrical conductivity of the gained condensate, nor the analysis of the vapor flow by optical methods show significant droplet entrainment, so there are no concerns regarding the purity of the produced condensate for the use as drinking water.

Keywords

Flash evaporation; Flash chamber design; Seawater desalination; Waste heat utilization; Solar thermal energy

2 Introduction

Almost a quarter of the worldwide installed desalination capacity is provided by systems with Multi Stage Flash evaporation (MSF). In terms of quantity, MSF is therefore the second most important process after Reverse Osmosis (RO) [1]. Especially in the Middle East and the North African region (MENA), where energy supply is based on oil deposits, thermal desalination processes such as MSF strongly predominate [2]. MSF technology is used in large-scale plants with capacities of up to 90,000 m³/d. The specific energy requirement of MSF plants is comparatively high, since in addition to the electrical energy requirement of 2.5 – 4 kWh/m³, a thermal energy requirement of 7.5 – 12 kWh/m³ must also be covered [3]. Thus, MSF plants are characterized by large space requirements and high investment and operation costs. Apart from the high energy demand, other environmental aspects need to be taken into account: large-scale seawater desalination plants show severe environmental impacts, mainly associated with the construction and operation of marine intake systems and the disposal of concentrated brines [4]. As highlighted in several studies, the use of renewable energy such as solar thermal energy is expected to play an important role in the future production of potable water by means of desalination in the MENA region [5],[6]. Addressing the sustainability of large-scale desalination plants, there are several approaches discussed in literature which deal with seawater desalination by the use of concentrated solar power coupled with a MSF or RO process [7],[8].

On the other hand, in rural areas, there is a need for smaller decentralized desalination plants which preferably are based on solar power utilization and allow for cheap and easy to handle water supply. Amongst others, Al-Kharabsheh et al. discuss a simple desalination process that uses low-grade solar heat [9]. Vacuum conditions in the condenser are provided by making use of geodetic height differences between the condenser and the water tanks. Thereby, the use of a conventional vacuum pump is avoided, and the need for auxiliary power is reduced to a minimum. They report a double yield of potable water if compared to a simple flat-basin solar still. Another approach to obtain passively created vacuum conditions for solar flash desalination is investigated with both experimental and simulation studies by Abutayeh et al. [10]. Muthanayagam et al. [11] describe another experimental approach for seawater desalination via flash evaporation. They suggest using seawater from different depths and thus different temperatures for feed and cooling water, respectively. Feed water enters the evaporator at a temperature of 26 – 32 °C and is nebulized by a swirl nozzle. Entrainment of droplets with the steam flow is prevented by using a demister unit. The temperature of the cooling water is given with 6 – 12 °C, which corresponds to seawater temperatures in high ocean depths. Experimental results at vaporization pressures of 13 – 24 hPa are reported to show satisfying agreement with a theoretical model. Muthanayagam et al. also report that they did not find a relation between the rate of condensation and the salt content of the feed water. Hence, many of their experiments were conducted with groundwater [12]. The influence of the direction of feed water injection on flash spray desalination was analyzed by Ikegami et al. [13]. They found a vertical, upward jet injection method with a tubular shaped nozzle to be suitable for compact and efficient spray flash desalination systems. Mutair et al. further analyzed the influencing parameters on flash evaporation from a superheated water jet when a nozzle is used [14].

The background of our work is a desalination process which is described in detail by Witt [15]. A schematic drawing of the complete desalination process is depicted in Fig. 1. This multi-effect process offers the supply of drinking water as well as of electrical energy. Hot water with a temperature of 70 – 95 °C is prepared in solar thermal collectors or by using low temperature waste heat. A high temperature water tank is used for thermal energy storage, e.g. if the production of potable water is needed during night or days with poor solar radiation. Vacuum steam is produced from the hot water by flash evaporation and afterwards expanded in a steam turbine. Additionally, the electrical energy produced by a generator can be used as auxiliary power to drive process components, but also for external applications. In a final step, all remaining vapor is being condensed with cold sea water, and the condensate is used to prepare drinking water. If the electricity gained from the steam turbine can be used for power supply of the desalination plant, this process can be conducted entirely self-sustaining, which presents great potential especially in rural areas.

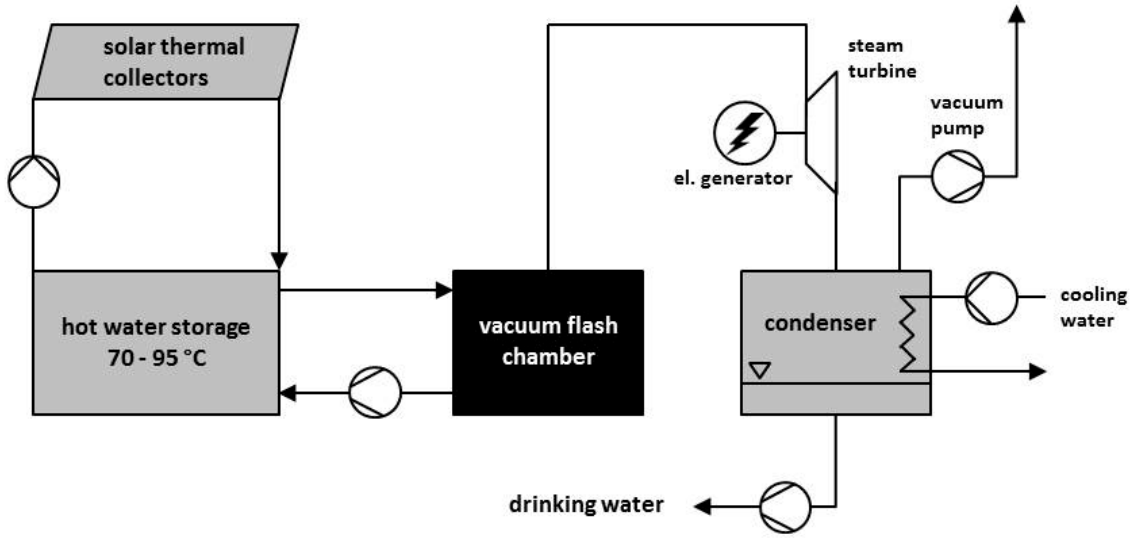

Fig. 1: Schematic flow diagram of a multi-effect solar desalination plant as proposed in [15].

In our study, a newly developed, both space and cost saving flash geometry is experimentally investigated. It uses standard process engineering components to achieve an efficient thermal desalination with no need to add pressure loss causing demisters. As, in contrast to standard evaporator geometries, there is no generally accepted engineering guideline available that describes how to design and dimension a flash evaporator, an extensive literature study on different flash chamber geometries was conducted.

Most of the flash evaporation concepts mentioned above share the fact that nozzles, f.e. swirl nozzles or tubular shaped nozzles, are used to inject the superheated water into a flash chamber and thereby make the evaporation process faster and more efficient. However, the application of a nozzle could present two major disadvantages if it comes to the flash evaporation of saline water: Firstly, nozzles with small diameters tend to plugging if crude seawater is used which would lead to either high maintenance effort or pretreatment of saline water. Secondly, spraying the liquid could cause the formation of tiny droplets of saline water which are carried along into the condenser by the vapor flow. Not only for vacuum spray

evaporation, but also in circulatory and stationary flash evaporation, brine entrainment is reported to be an issue. In a simple flash chamber with a tubular feed inlet, Zhang et al. observed strong steam-carrying effects especially when the inlet superheat increased [16]. This could not only lead to contamination of the condensate, i.e. the drinking water, but in addition cause damage on the steam turbine blades of multi-effect desalination plants. Therefore, the use of a demister unit is required to separate the droplets from the steam. A demister on the other hand leads to pressure loss and for this reason decreases the work gained in the turbine and thus the output of electrical energy.

A quite similar problem occurs in a very different technological area: in geothermic power generation, turbines are reported to fail because of droplet entrainment and mineral carriage with the steam. To ensure that only dry and clean steam enters the turbine, special geometries of liquid-vapor separators are used, which show separation efficiencies of 99.9% or even higher [17]. One type commonly used is a vertical cyclone separator with top or bottom outlet [18]. For these types of separators, which operate at high steam throughputs, the effectiveness of droplet separation is strongly influenced by the inlet flow velocity: for low velocities, poor separation is observed. Increasing the velocity increases the effectiveness of separation and thus leads to smaller equipment sizes, but, at high input velocities, a breakdown point is reached. As of this moment, the wetness of the output flow increases significantly when further increasing the input velocity [19].

In the current work, a flash chamber design is implemented and experimentally analyzed that combines both the function of a flash evaporator as well as of a vertical gas-liquid separator with low pressure drop into one process component. It is designed in a way that allows for easy and cheap maintenance and low investment costs. In the presented experimental study, hot water is produced with electrical power instead of solar energy for experimental reasons. Furthermore, the condenser is replaced by a liquid ring vacuum pump to establish and adjust the investigated vacuum pressures.

3 Experimental setup and procedure

An experimental setup was designed that allows investigations on the kinetics of flash evaporation of water. In principle, there are two functions to be fulfilled by the evaporator: complete evaporation in terms of thermodynamic equilibrium conditions, and phase separation between the gas and the liquid phase. We suggest a novel design that combines both of these two functions into one single component. Hence, the main question to be addressed is whether any formation of droplets can be observed during the flash process, and, if so, how the flash chamber performs in separating the droplets from the water vapor. This is of high importance regarding the later desalination process as mentioned above: droplets carried by the vapor stream may damage the steam turbine and contaminate the condensate which will serve as drinking water. For this reason, the design of the evaporation chamber is optimized to achieve the above mentioned requirements. The setup is operated with a maximum feed of 1,600 liters of water per hour.

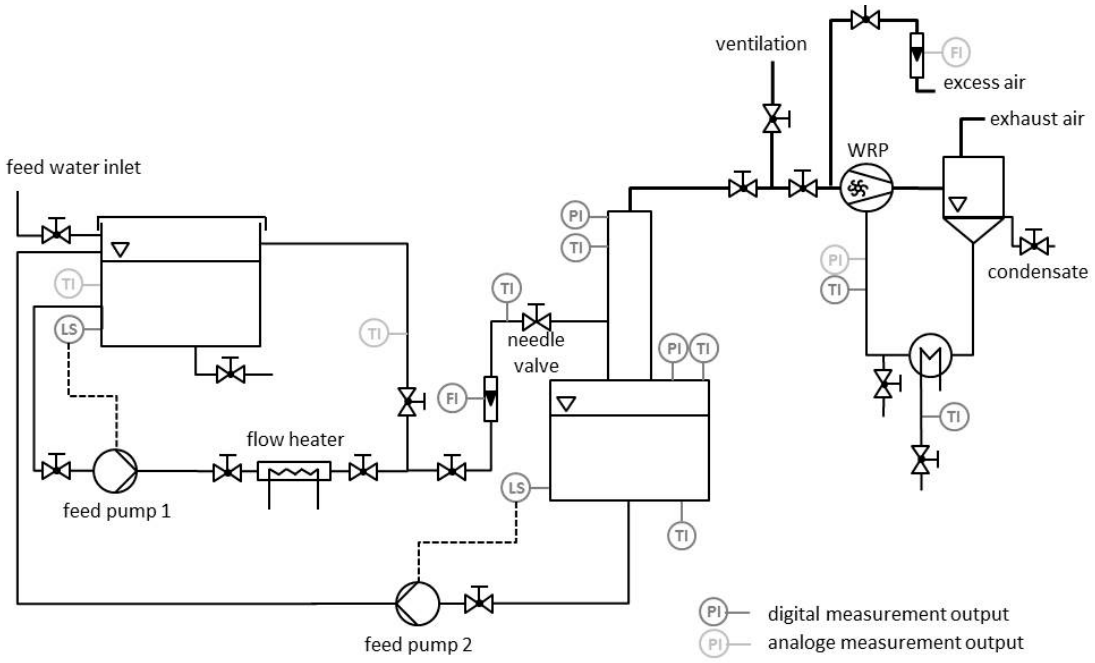

Fig. 2: Flow scheme of the experimental setup.

Fig. 2 shows a schematic diagram of the laboratory test rig. The setup consists of three main parts: first, the hot water preparation module (which will later be replaced by solar thermal collectors), second, the flash evaporator, and third, a water ring vacuum pump (WRP) that represents the condenser. Variable operating parameters are the temperature and the flow rate of the input flow (60 – 90 °C, 500 – 1,600 l/h) as well as the vacuum pressure in the flash chamber (180 – 400 hPa).

As Muthunayagam et al. report that their experimental findings on the rate of evaporation indicated no dependency on the salt content of the feed water [12], first experiments in the present work were conducted with tap water. Further experiments were carried out with increasing contents of salt with up to 100 grams per liter (in means of sodium chloride) to show the effect on the quality of the product. Typically, seawater as feed for desalination processes contains about 35 grams of salt per liter.

The novel design of the flash chamber includes a needle valve as expansion device and a vertical tube to separate the vapor-liquid-mixture into steam and concentrated liquid. The cylinder-shaped head of the evaporator is made of borosilicate glass to allow monitoring droplet formation and separation. The diameter of the glass tube is set to 200 mm (see Fig. 3a) and 100 mm, respectively, to realize higher gas velocities for further experimental studies. The glass part is separated into two sections by a segment made of stainless steel. Feed water enters the flash chamber within this section via a tube with an inner diameter of 40 mm. The lower part of the setup contains a vessel made of polypropylene. It is used for collecting the remaining liquid as the laboratory experiment is conducted as a batch process. The total height of the 200 mm flash evaporator is 2,300 mm, with the essential components for evaporation and gas-liquid separation only being 850 mm tall, as depicted in Fig. 3a. The upper glass section of the 100 mm flash evaporator has a height of 400 mm. The setup is equipped with several temperature and pressure sensors. Their location is shown in Fig. 3b.

Resistance temperature detectors of the type Pt100 with an accuracy ± 0.5 K of were used. The error of the pressure sensors is ± 0.5 % of the full measurement scale (0.1 MPa), and the uncertainty of the volume flow meter is in the range of ± 0.5 % of the measured value.

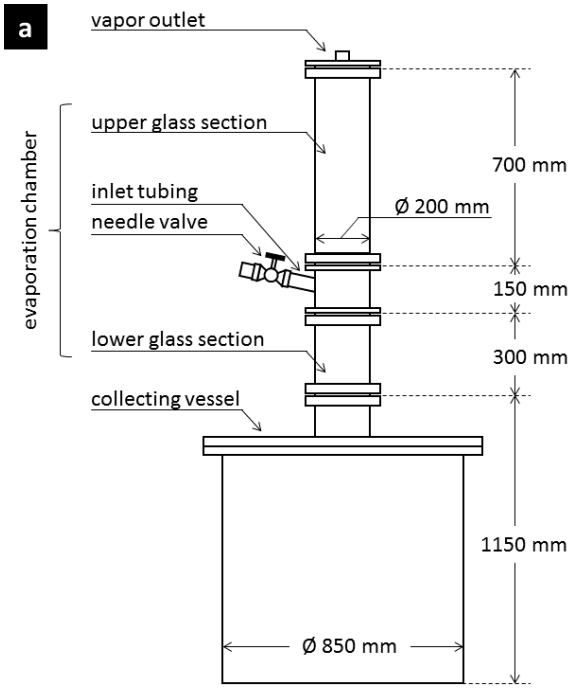

Fig. 3a: Design drawing of the flash chamber.

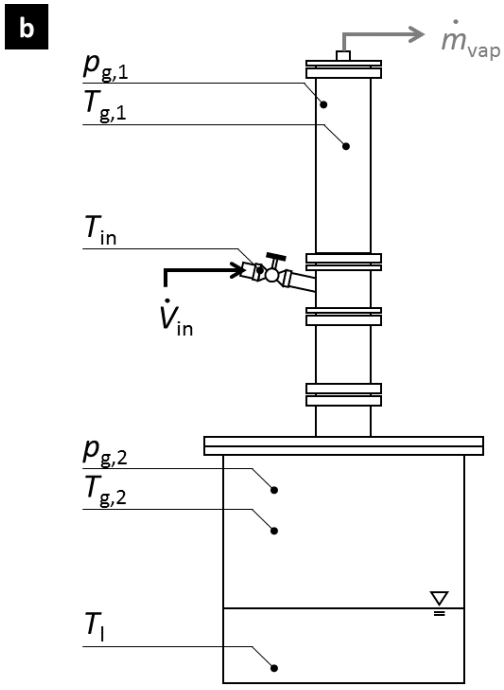

Fig. 3b: Position of measurement points.

3.1 Conceptual design of the flash evaporator

After the feed flow passes the needle valve where the pressure drop from ambient pressure to vacuum conditions and thus flash evaporation takes place, the two phase flow enters a small inlet tube with a length of about 250 mm. This tube is connected to the evaporation device tangentially with respect to the diameter of the separation tube (vertical column). The nose of the inlet tube points downwards to lead the liquid flow towards the lower end of the separation column. The end of the tube is cut in an angle of 35° and twisted in a way that drops are prevented from bouncing upwards. Measured from the inlet position to the top of the setup, the effective separation height of the 200 mm diameter flash column is 750 mm. The inlet section with the downwards pointing tube is shown in Fig. 4a and Fig. 4b. The inlet tube geometry for the smaller 100 mm diameter evaporation chamber is designed similarly. Here, the resulting effective separation height of the evaporation chamber is 500 mm.

Fig. 4a: Adjustment of the inlet tube to the separation chamber (200 mm diameter).

Fig. 4b: Twisted and tangential mounting of the inlet tube.

The determination of the flash chamber's diameter is based on the following considerations: the steam volume flow determines the flow velocity, with which the steam in the flash chamber moves upwards for a given tube diameter. The faster the steam, the smaller are the droplets carried along with the gas. For the design of the evaporator, the decisive factor is the consideration from which droplet diameter liquid droplets are not carried by the gas flow but instead are stripped off due to the gravitational force. This does not only apply to fine droplets formed by the sudden evaporation, but also to droplets forming when the liquid flow hits the column surface. Centrifugal forces provoke that large droplets are separated from the steam at the very inlet into the evaporation chamber, and therefore, the following considerations refer to smaller droplets which follow the gas flow in axial direction.

It is assumed that no evaporation or condensation occurs at the droplet surface, and therefore the droplet mass is constant. A droplet is separated from a gas stream by gravitation if the gravitational force exceeds the sum of flow resistance force and buoyant force. It is further assumed that the buoyant force is negligibly small compared to the gravitational force because the density of the displaced gas is significantly smaller than the density of the liquid. In addition, the initial speed of the droplet is assumed to be irrelevant as the height of the flash chamber is comparatively large. The flow resistance force F_d and the gravitational force F_g as a function of the droplet diameter are shown in Fig. 5 for an evaporator diameter of 200 mm. The diameter of a droplet just being separated ($d_{droplet}$*) is found to be 0.27 mm (marked by the vertical line). Droplets with larger diameters are stripped off the steam, and smaller droplets are entrained by the gas flow. Plotting the limit diameters against the vapor's superficial (or empty tube) velocity, as depicted in Fig. 6, reveals that larger evaporator diameters are better suited for the separation of smaller droplets due to the lower superficial velocity than smaller evaporator diameters. A higher superficial velocity v_{mean} of the steam therefore results in a larger limit diameter $d_{droplet}$*. Depending on the evaporator diameter, droplet Reynolds numbers are in the range of $Re = 3 – 51$ for the different superficial velocities. Thus, the approximation equation for the transition area according to Kuerten et al. is used [20].

In these considerations, several simplifying assumptions are made: the equations described above for calculating the flow resistance coefficients apply to the inflow of ideally spherical, smooth, and solid particles. Since the expected droplet diameters are very small, it is assumed that due to the high surface tension of water, the droplets are not deformed but retain a

spherical shape [20]. Another assumption of our approach is that the flow, in which the droplets move, forms a laminar flow profile. Even for the given test conditions with the larger evaporation tube with 200 mm diameter, however, Reynolds numbers for empty tube flow lie in the transition regime between laminar and turbulent flow. Therefore, the results depicted in Fig. 5 and Fig. 6 can only be evaluated qualitatively.

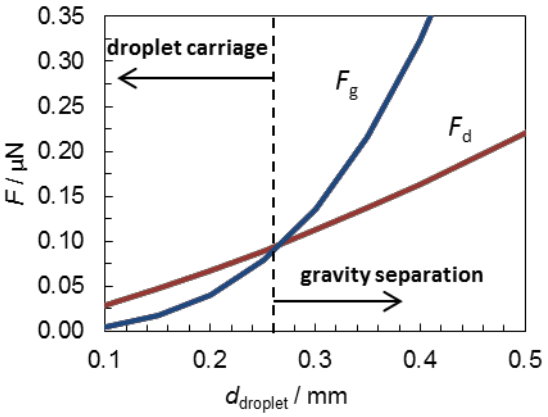

Fig. 5: Forces occurring at the droplet as a function of droplet size in an evaporation tube with a diameter of 200 mm (feed flow 1000 l/h, feed temperature 90 °C, vapor content 4.48 %).

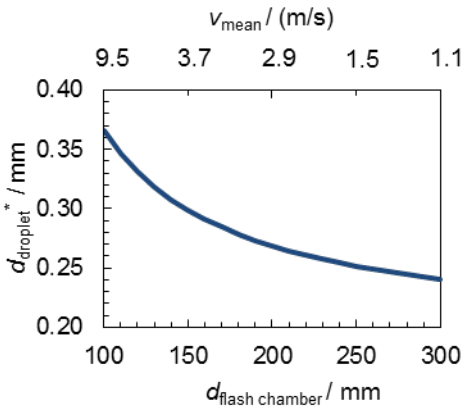

Fig. 6: Diameter of a droplet size that is just being separated from the steam flow by gravity as a function of tube diameter and the steam's mean empty tube velocity.

So far, is not known if and to what extent abrupt evaporation of water forms droplets when sprayed into an evacuated container, and which droplet sizes are to be expected. Based on the discussed considerations, evaporator tubes with a diameter of 100 mm and 200 mm were chosen for this experimental study. The proposed compact flash evaporator design offers the major advantage of a minimized pressure loss due to an efficient gas-liquid-separation as there is no further need to use demisters or similar components to filter small droplets.

3.2 Experimental procedure

With the setup described above, experiments to prove the feasibility of the novel evaporation chamber design for water desalination were carried out. The expected vapor content is calculated from the given temperature of the liquid inlet flow and pressure in the flash chamber according to an energy balance of the isenthalpic expansion process. Thermodynamic equilibrium conditions define the maximum vapor content that can be reached. In a parameter study, experimental results were evaluated in comparison to these calculations. Estimating the error propagation for the vapor content results in a maximum deviation of ± 0.6 % for the vapor content calculated from experimental data.

To rate the influence of the operation parameters, different test series were performed. All conducted experiments followed this procedure: Water is heated in the storage tank with (max. content 340 liters) to a temperature of 60 – 90 °C. The hot inlet flow is pumped into the flash chamber with the volume flow being regulated by the needle valve in a range of 500 – 1,600 l/h. To set initial conditions in the flash chamber and to maintain vacuum pressure

during the experiment, it is evacuated by means of a water ring vacuum pump before starting the experiment. The temperature of its operating liquid ring water sets the limit for the minimal pressure that can be maintained. As the pump only offers a constant revolution speed, the desired vacuum pressure has to be adjusted by regulating the amount of excess air into the pumps' inflow stream. The water ring vacuum pump furthermore operates as vapor condenser. For dissipating the condensation enthalpy, the pump is chilled with cooling water. The generated condensate constantly leaves the pump during the experiment, and its weight is measured after the end of the experiment. This value is used to evaluate the experimental yield of water produced in comparison to its theoretical value. The experiments were conducted batch-wise, and the experimental time varied between 10 and 30 minutes depending on the installed feed volume flow.

3.3 Detection of droplet entrainment

Droplet formation can occur due to flash effects during evaporation or due to mechanical reasons, e.g. at the tubular inlet of the flash chamber. To evaluate the flash chamber's performance as a gas-liquid gravity separator, two different types of measurements are conducted. On the one hand, an optical measurement device is installed. It offers the exposure of droplets to a conventional CCD camera by illuminating with dual-color flash light. This allows not only a qualitative but also a quantitative analysis of the droplet number as well as for investigations on the dynamics of droplet movement. On the other hand, conductivity measurements of the condensate are performed. Droplets carried by the vapor steam result in an increased conductivity of the condensate, which is gathered in the water ring pump. This allows a quantitative calculation of the volume flow of droplet entrainment by balancing the salt masses.

3.3.1 Calculation based on electrical conductivity measurements

The principle of droplet detection via electrical conductivity measurements is based on conductivity differences between aqueous solutions of sodium chloride. Salinized feed water shows an experimental electrical conductivity in the range of 650-665 µS/cm (regular tap water), to 125,000 µS/cm (concentrated salt water). As the process water of the liquid ring vacuum pump, which is drained before the start of an experiment and replaced by deionized water, has a significantly lower conductivity (2-3 µS/cm), droplet entrainment from the feed inlet results in a higher electrical conductivity of the process water. On the other hand, condensation of pure water vapor decreases the conductivity of the operating liquid.

Although several simplifications are made, the following analysis offers a well estimation for the quality of gas-liquid separation. In our mass balance model, the water ring vacuum pump is assumed to be an ideal stirred tank with constant volume. Thus, the output volume flow (overflow of process water) equals the input volume flow (water vapor condensate). Hence, the molar mass balance for the salt content in the operating liquid is given by

$$\frac{\mathrm{d}N_{\mathrm{salt}}(t)}{\mathrm{d}t} = \dot{N}_{\mathrm{salt,\,vapor}} + \dot{N}_{\mathrm{salt,\,droplet}} - \dot{N}_{\mathrm{salt,\,outflow}}, \quad (1)$$

with $\frac{\mathrm{d}N_{\mathrm{salt}}(t)}{\mathrm{d}t}$ being the change of the amount of salt inside the liquid ring pump with respect to time. Noted with volume flows ($\dot{V}$) and salt concentrations (c), eq. (1) results in

$$\frac{\mathrm{d}N_{\mathrm{salt}}(t)}{\mathrm{d}t} = \dot{V}_{\mathrm{vapor}} \cdot c_{\mathrm{salt,vapor}} + \dot{V}_{\mathrm{entrainment}} \cdot c_{\mathrm{salt,droplet}} - \dot{V}_{\mathrm{out}} \cdot c_{\mathrm{salt,opliq}}(t)\,. \quad (2)$$

With $c_{\mathrm{salt,opliq}}(t)$ being the salt concentration of the operating liquid and $c_{\mathrm{salt,vapor}} = 0\,\frac{g}{l}$ the salt concentration of the pure vapor, the upper equation is simplified to the expression

$$V_{\mathrm{o}}\,\frac{\mathrm{d}c_{\mathrm{salt}}(t)}{\mathrm{d}t} = \dot{V}_{\mathrm{entrainment}} \cdot c_{\mathrm{salt,droplet}} - \dot{V}_{\mathrm{out}} \cdot c_{\mathrm{salt,opliq}}(t)\,. \quad (3)$$

In this equation, V_{o} is the volume of the operating liquid, which stays at a constant number.

The integration of eq. (3) in the limits of the experiment's start and end according to the experimental time and salt concentration in the operating ring pump water, we derive the following equation for the volume flow of droplet entrainment:

$$\dot{V}_{\mathrm{entrainment}} = \frac{V_{\mathrm{out}}}{t_{\mathrm{end}}} \cdot \frac{c^{\mathrm{end}}_{\mathrm{salt,opliq}} - c^{\mathrm{start}}_{\mathrm{salt,opliq}} \cdot \exp\left\{-\frac{V_{\mathrm{out}}}{V_0}\right\}}{\left(1 - \exp\left\{-\frac{V_{\mathrm{out}}}{V_0}\right\}\right) \cdot c_{\mathrm{salt,doplet}}} \quad (4)$$

Here, V_{out} is the entire volume of process water leaving the water ring pump during the measurement, and $c_{\mathrm{salt,opliq}}$ is the concentration of the feed water. Each parameter in this final equation is determined experimentally. The salt concentration is derived from the electrical conductivities measurements as for low sodium chloride concentrations, a linear correlation between conductivity and concentration can be assumed [21]. Electrical conductivities were measured with a sensor accuracy of ± 0.5 % of the measured values in mS/cm. The maximum error based on error propagation for the salt mass analysis results in a maximal uncertainty of ± 2 ml/l considering all measurement accuracies.

3.3.2 Optical method

A standard reflex camera connected to a high precision flash system (Nano-Twin-Flash device from *High-Speed Photo-Systeme*, Germany) is used to optically detect droplets in different locations within the evaporation chamber. The camera's focal length is adjusted to different spots along the height and the depth of the glass column above the tubular feed inlet as depicted in Fig. 7.

Two 25 ns light flashes of different colors are triggered with an adjustable delay time, and a photo is taken with an exposure time that exceeds this delay. If a moving droplet is exposed twice in one shot, it casts two differently colored images on the CCD sensor that allow for analyzing the speed and the direction of the droplet movement. In the experiments presented, red and green filters are used for the first and the second flash, respectively. Overlap of the two flashes into a single picture results in a yellowish color of the final image. A red dot shows the position of the droplet during the first flash (as the green light does not reach the optical sensor), and a green dot its' position at the second point of time. Only if the delay time between the two flashes is too short for the droplets to cover a certain distance, the two positions overlap, and thus are marked by a single dark spot as no light reaches the CCD sensor.

The flashes expose an area with a diameter of 25 mm. To receive a clear view of the droplets, it is necessary to avoid condensation on the glass wall of the evaporation chamber as well as formation of mist, as this would cause blurred images. For this use, additional heating by fans and a heating collar is installed on the outer glass wall whenever optical measurements are conducted during the series of experiments.

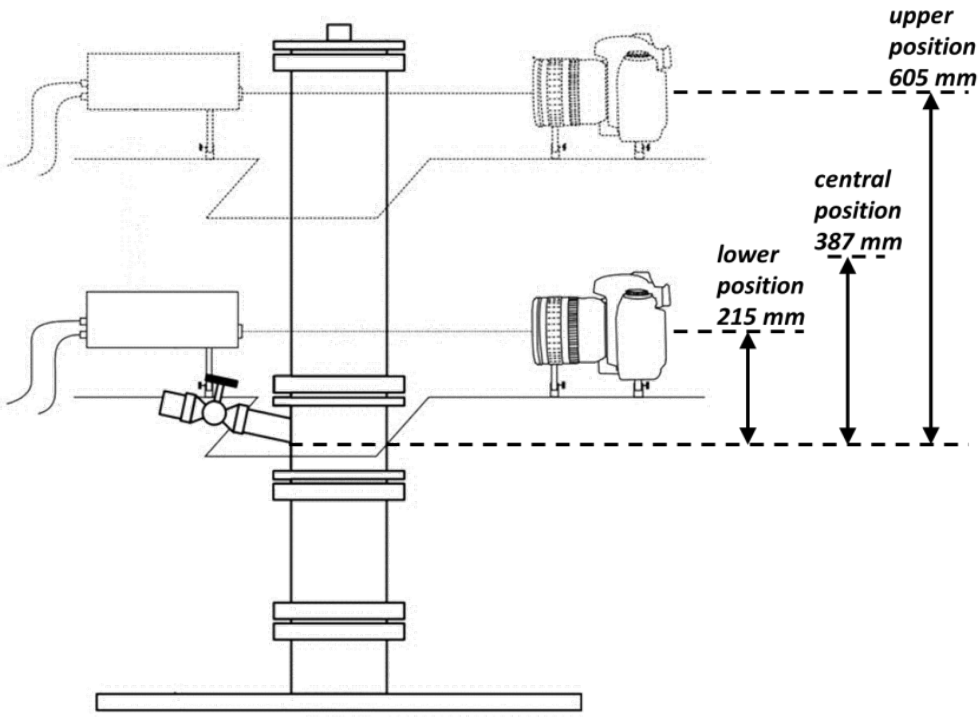

Fig. 7: Adjustment of the CCD camera and the flash system to the evaporation chamber. Figure adapted from [22].

4 Results and Discussion

In the following section, the experimental results are presented in three parts: At first, results on temperature and pressure progression in the flash chamber are reported. Afterwards, the evaporation yield and the entrainment of droplets with the steam flow are discussed.

4.1 Temperature and pressure profiles

Experiments at different feed volume flows and temperatures as well as flash chamber pressures have been performed to assess the evaporation performance under steady state conditions. Pressure sensors at the bottom and at the top of the flash chamber showed concordant values, as pressure drop due to built-in components is negligibly small. Therefore, only the pressure profile measured with the sensor that is mounted further down in the evaporation chamber ($p_{g,2}$, see Fig. 3b) is depicted in the following graphs.

Fig. 8a shows data from an experiment with a feed flow rate of 1000 l/h and a feed temperature of 70 °C. The evaporation chamber is evacuated to a minimum pressure of 150 hPa. In Fig. 8b, corresponding temperature curves are shown. After few minutes, the temperature sensors $T_{g,1}$ and $T_{g,2}$, all of which are in the gas phase at this point, display

ambient conditions. At about t = 18 min, the needle valve is opened and the volumetric flow which is measured by the rotameter jumps up to the target value. The experiment runs for 16 minutes until the hot water reservoir is fully discharged. The flash pressure reaches 240 hPa during the experiment. Considering the actual pressure trend, the corresponding saturation temperatures are calculated (T_{sat}). Both the temperature sensors in the gas phase as well as the sensor mounted in the liquid phase show congruent values that match the expected saturation temperature. Based on these observations it is concluded that thermodynamic equilibrium conditions are reached.

As the collecting vessel was not emptied before the start of experiment, it contains remaining warm water from a preceding experimental run. For this reason, the temperature in the liquid reservoir does not start at ambient level. However, this does not have any further impact on the subsequent temperature and pressure profiles.

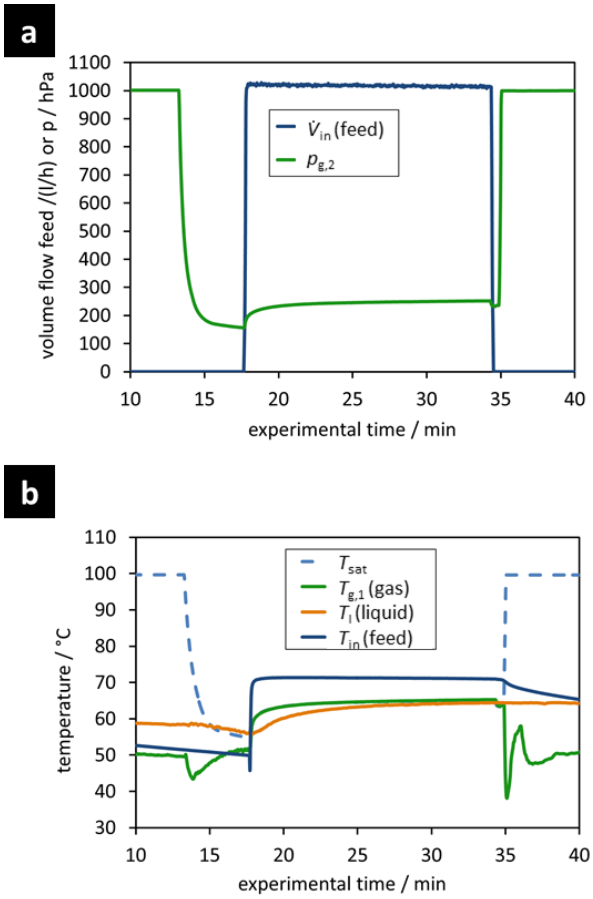

Fig.8a: Evaporation experiment with $\dot{V}_{feed} = 1000\,\frac{l}{h}$, $T_{feed} = 70$ °C, $p_{flash} =$ 240 hPa, and a flash column diameter of 200 mm. Fig.8b: Corresponding temperature curves.

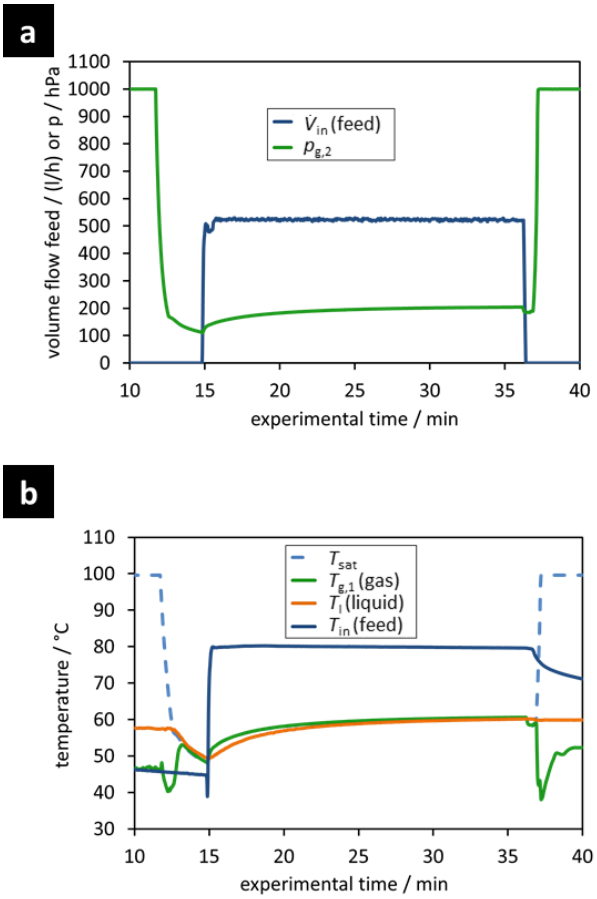

Fig. 9a: Evaporation experiment with $\dot{V}_{feed} = 520\,\frac{l}{h}$, $T_{feed} = 80$ °C, $p_{flash} =$ 200 hPa, and a flash column diameter of 200 mm. Fig. 9b: Corresponding temperature curves.

Fig. 9a and b show the temperature and pressure profiles for a flash experiment with half of the feed volume flow, a higher liquid temperature of 80 °C, and a lower flash pressure of 200 hPa compared to Fig. 8. All the curves show analogous behavior as before. The experimental time was increased by decreasing the volume flow controlled by the needle valve. Although the temperature step of the flash is increased from 5 K to 20 K, steady state conditions were reached.

The limit of the experimental range of steady conditions had been outreached if a continuous pressure increase during an experiment would have been observed. This occurred in some experiments with high feed temperatures and volume flows, and was caused by a lack of cooling duty at the vacuum pump: the temperature of its operating water increased significantly due to the release of condensation enthalpy, and the capacity of the heat exchanger was not sufficient to dissipate the surplus heat.

Both of the experiments presented in Fig. 8 and Fig. 9 were conducted with tap water as feed stream. Whereas during the measurement presented in Fig. 8, the amount of produced desalinated water was 2.2 kg, here 5.5 kg of condensate was collected. This difference depends on the higher liquid temperature and lower flash pressure, which will be discussed in the next chapter.

4.2 Evaporation yield

Maximum product quantity is received when a vapor content according to the thermodynamic equilibrium is reached. These values are calculated based on the isenthalpic process of flash evaporation and vary between 0.5 % and 4.5 % of the liquid mass flowing through the expansion valve. They are dominated by the liquid temperature before the expansion and the flash chamber pressure: by rising the liquid temperature and decreasing the flash pressure the vapor content is increasing. The change in kinetic energy due to a phase change from liquid to gas phase where the latter one has a higher velocity compared to the liquid phase has a comparably low impact on the vapor content. It changes the value in the vapor content in the fourth position after the decimal point for the used experimental geometry when calculated with the highest volume flow.

The results of the vapor yield for all experiments with varying feed volume flow, salt content, feed temperature, and flash pressure are presented in Fig. 10. Here, the experimental vapor yield is plotted versus the theoretical one. The bisecting line gives ideal experimental results which reach theoretical values according to the thermodynamic equilibrium.

Evaporation yield or evaporation efficiency can be defined as the ratio of experimental and theoretical steam contents that are expected for given feed temperatures and flash pressures. In the presented series of experiments, heat isolation is found to have a high impact on the evaporation efficiency, as condensation on the walls of the evaporation chamber plays an essential role. The data points depicted in Fig. 10 and Fig. 11 are retrieved from experiments with the test setup not being thermally insulated against the ambient. Fig. 11 shows the comparison between measurements with the two different flash chamber diameters. On the one hand, the superficial velocity of the steam is higher by the factor of 4 for the smaller tube diameter, which results in a larger theoretical limit droplet diameter and thus enhanced droplet

entrainment. On the other hand, a smaller chamber diameter goes along with a lower surface area, which reduces steam condensation on cold walls of the evaporation chamber. In addition, the separation height of the flash chamber is significantly reduced for the 100 mm evaporator diameter (from 750 mm to 500 mm, measured from the inlet position to the top). However, no significant performance difference regarding effective gas-liquid separation is observed for the 200 mm diameter tube compared to the 100 mm diameter flash chamber.

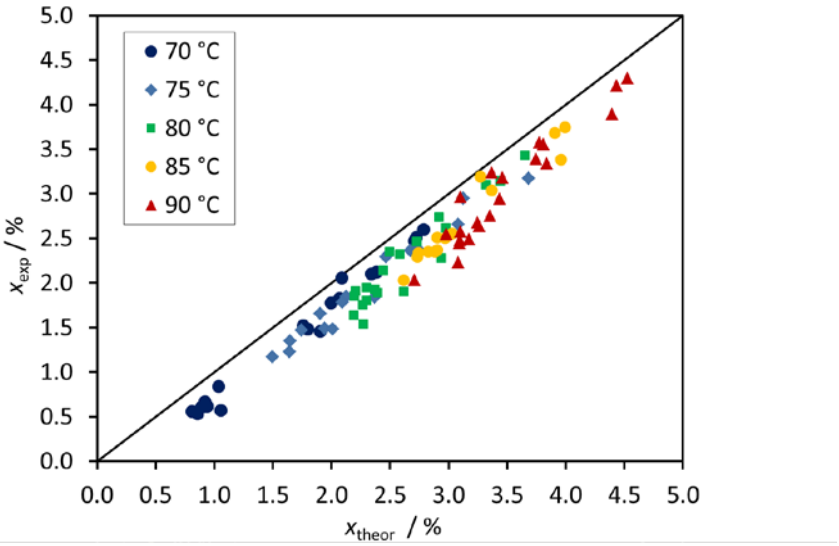

Fig. 10: Experimental vapor content versus theoretical vapor yield according to isenthalpic flash evaporation process for varying feed temperatures and volume flows, column diameters of 200 mm and 100 mm, and salt concentrations between regular tap water and 120 g NaCl/l.

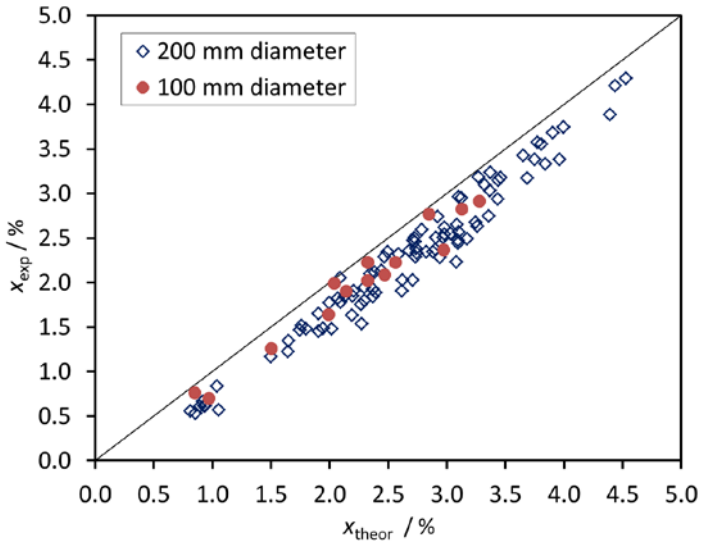

Fig. 11: Comparison between different tube diameters according to the experimental vapor content for varying feed temperatures and volume flows, and salt concentrations between regular tap water and 120 g NaCl/l.

The ratio of experimental and theoretical vapor contents results in values in the range of 54 % up to 98 % for all analyzed measurements. Best results are achieved with medium feed temperatures and medium flow rates. All in all, the experimental results prove satisfying evaporation efficiency. To reach highest vapor yields, cold spots in future plants need to be avoided by minimizing the geometry or by thermal insulation.

4.3 Purity of condensate

For feed flow temperatures of 70 °C and a variation of the pressure in the flash chamber, the results of the conductivity measurements are presented in Tab. 1. The feed volume flow in these measurements was fixed at 1000 l/h. The amount of droplet entrainment is evaluated according to the mass balances described in section 3.3.1, and is based on a constant operation water volume of 9.5 liters in the liquid ring vacuum pump [22].

Tab. 1: Results of conductivity measurements and resulting volume flow of droplet entrainment for a feed temperature of 70 °C, and different time-averaged flash chamber pressures at 1000 l/h liquid feed (chamber diameter 200 mm, separation height 750 mm).

p_{flash} (hPa)	V_{cond} (l)	t_{exp} (min)	$\dot{V}_{entr.}$ (ml/min)	$\frac{\dot{V}_{entr.}}{\dot{V}_{cond}}$ (%)
169	4.0	17.9	4.2	1.9
187	4.5	17.9	3.9	1.6
200	3.9	17.2	3.7	1.6
218	2.8	17.0	3.2	1.9
242	2.2	16.8	2.7	2.0

For all the experiments, regular tap water is used as feed. Droplet entrainment is found to account for 2 % maximum of the total amount of condensate. However, no correlation between the pressure in the flash chamber and the intensity of entrainment is observed. Only if the feed temperature is increased to 90 °C, droplet entrainment is boosted, see Tab. 2. In this series of experiments, the feed flow rate is varied in the range from 500 l/h to 1000 l/h and the salt concentration of the feed water shows values of regular tap water. No coherent relationship between droplet entrainment and the feed flow rate is found.

Tab. 2: Results of conductivity measurements and resulting volume flow of droplet entrainment for a feed temperature of 90 °C, and different time-averaged flash chamber pressures and feed flow rates (chamber diameter 200 mm, separation height 750 mm).

$\dot{V}_{feed}$ (l/h)	p_{flash} (hPa)	V_{cond} (l)	t_{exp} (min)	$\dot{V}_{entr.}$ (ml/min)	$\frac{\dot{V}_{entr.}}{\dot{V}_{cond}}$ (%)
1005	300	7.4	21.7	10.4	3.1
997	240	9.3	20.4	13.9	3.0
720	290	10.9	28.8	12.3	3.2
497	310	11.5	36.5	10.1	3.2

Due to the simplifying assumptions in the calculation method, these results can only be interpreted qualitatively. Still, from the experimental results we conclude that droplet entrainment does not play a major role regarding the conductivity analysis of the condensate. A similar result was found for the experiments with the smaller evaporation chamber diameter

and reduced separation height (chamber diameter 100 mm, separation height 500 mm). For initial salt contents of 115 g/l, a condensate salt concentration in the range of 0.08 g/l was found for the smaller test setup. In comparison, in the experiments with the larger test setup (chamber diameter 200 mm, separation height 750 mm), the mean salt concentration in the condensate was found to be 0.04 g/l for an average initial salt content of 53 g/l. In analogy to the previously discussed measurement evaluation on the evaporation yield, no quantitative statement can be made as to which design performs better regarding efficient gas-liquid separation.

Further experimental data with changing feed volume flows, flash pressures and feed salt concentrations up to 120 g NaCl/l confirmed the observation of efficient gas-liquid separation. This finding is supported by the results of the optical evaluation method, which are described in the following.

The images that were taken with the Nano-Twin-Flash setup during the experiments were compared to each other regarding the height along the flash chamber's vertical axis as well as regarding the depth in which they were taken. It is found that a lot of droplets occur in the area right above the tubular inlet of the two-phase flow into the evaporation chamber. The number of droplets decreased with increasing horizontal distance between the object plane and the inlet. It is assumed that many droplets are formed because of mechanical forces when the liquid flow hits the wall of the evaporation chamber. As it can be seen in the photographs of the two-phase flow entering the evaporation chamber in Fig. 12, this effect is also visible to the naked eye to a varying degree. Furthermore, the feed temperature increase results in a higher mean velocity of the two-phase flow due to the larger vapor content. The higher flow velocity goes along with the observed motion blur in Fig. 12b.

Fig. 12a: Two-phase flow at a feed temperature of 70 °C and a flow rate of 1011 l/h or 0.267 kg/s (200 mm chamber diameter; exposure time: 1/60 s).

Fig. 12b: Two-phase flow at a feed temperature of 90 °C and a flow rate of 982 l/h or 0.271 kg/s (200 mm chamber diameter; exposure time: 1/60 s).

If the distance to the inlet is increased in the vertical direction, the number of droplets that are detected via the double flash method decreases, see Fig. 13: in the left photograph, a lot of droplets are detected by the flash device, whereas the number is reduced in the higher position of the tube and disappears entirely at the top position of the column.

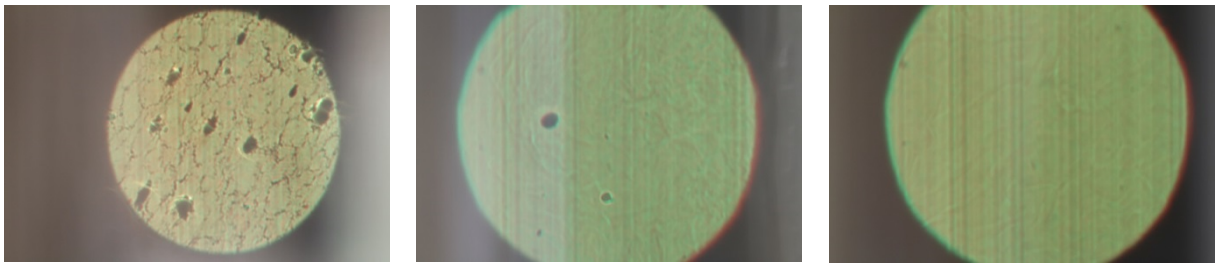

H = 215 mm H = 387 mm H = 605 mm

Fig 13: Optical measurements of droplets depending on the column height over inlet position for the same measurement parameters chosen.

Exemplarily, Fig. 14 shows a magnified section of an image that was taken during a flash experiment. The photograph on the left side reveals the entire section of 25 mm diameter that is exposed by the Nano-twin-Flash. Droplets are not visible to the naked eye. When zooming into the chosen section, the evaluation of the photograph indicates two droplets moving upwards. Optical analysis of this image reveals that the smaller droplet on the right has a diameter of roughly 50 µm whereas the larger droplet has a diameter of 130 µm. The delay time between the two flashes was set to 10 ms, the droplets therefore move with a velocity of 70 mm/s.

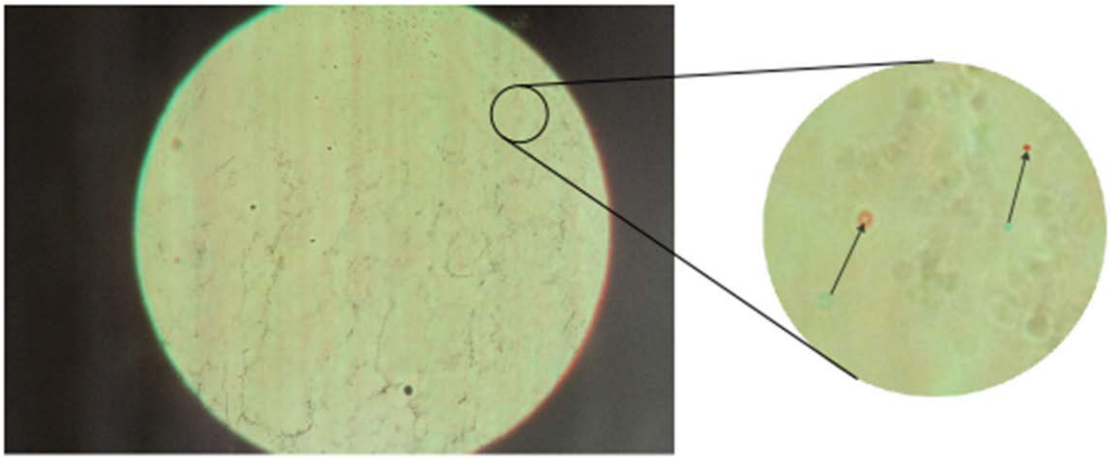

Fig. 14: Double-exposed image (delay time 10 ms, exposure time 77 ms, aperture 3.5).

5 Conclusions

In this work, a novel flash evaporator design is proposed which offers significant advancements compared to conventional evaporators used for seawater desalination such as a space efficient and cost saving construction. Due to the lack of a generally accepted guideline for the construction of flash evaporators in literature, a series of experiments was performed to develop design rules for evaporative expansion. All of these experiments support the successful proof of concept. The performed experiments are divided into two sections: Firstly, a parameter study was conducted to analyze different operation conditions and their impact on the evaporation yield. Secondly, the effectiveness of phase separation between the vapor and the remaining liquid was evaluated by optical measurements and an analysis based on conductivity measurements. The operating parameters such as the volume flow, flash pressure

and flash temperature, respectively, as well as the salt concentration were varied in a wide range to confirm the results.

The experimental results show that thermodynamic equilibrium is reached during flash evaporation. This conclusion is drawn from the temperatures and pressures that are observed in the flash chamber: both the temperatures in the gas phase as well as in the remaining liquid match the expected values, i.e., the saturation temperature calculated from the current flash pressure. However, the experimental evaporation efficiency which is determined by a mass balance does not catch the value that is expected from a theoretical calculation. Instead, it shows a deviation of about 15 % on average. It is assumed that this discrepancy originates from condensation on the walls of the flash chamber and the vessel due to heat losses to the ambient. Experimental and theoretical evaporation yields show satisfying agreement if the experiments are conducted at steady state, i.e. at constant flash pressure. Due to experimental constraints of the given test setup, this condition can only be experimentally fulfilled for low theoretical steam contents.

To examine the number of liquid droplets that are carried into the condenser by the vapor stream, a mass balance at the water ring pump combined with conductivity measurements was performed. Results of the conductivity measurements show that the carried droplets sum up to less than 2 % of the condensate for a 70 °C feed temperature, which is below measurement accuracy. In agreement with these results, testing by means of optical measurements does not show significant droplet entrainment in the upper part of the flash chamber.

It is concluded that the novel flash chamber with its compact design based on standard process technology equipment shows efficient evaporative expansion and accurate gas-liquid-separation with minimal droplet entrainment. Moreover, what sets this design apart from other technologies is the fact that there is no need to install an additional demister unit. As a result, high pressure losses are avoided with this chamber geometry. In addition, the setup contains no nozzles or other bottlenecks with small diameters which tend to plugging if crude seawater is used which would lead to either high maintenance effort or pretreatment of saline water. With the presented pilot plant, it is demonstrated that even for high salt concentrations the thermal desalination process works properly to treat sea or waste water by simple means. Moreover, as the required feed flow temperature does not exceed 90 °C, the needed thermal energy can be supplied by with solar thermal power or low-temperature waste heat.

The quantitative analysis of droplet entrainment for high sodium chloride concentrations (120 g/l) in the feed water is part of our ongoing experimental work. Moreover, a detailed analysis for smaller flash chamber diameters and heights will be conducted. Future work will focus on a further optimization of the flash chamber concerning its limits in size for pure water production and the extension on several flash stages to further increase the water production yield related to the feed volume flow.

6 Acknowledgements

The authors wish to thank Andreas Albrecht and Eduardo Jose Hanna Hernandez for their contribution in experimental work. Besides, the authors wish to thank Michael Witt for providing basic understanding of the challenges in renewable seawater desalination as well as parts of the experimental infrastructure, and gratefully acknowledge the financial support from the "Bundesministerium für Bildung und Forschung" (BMBF, Federal Ministry of Education and Research, Germany).

7 References

[1] S. Miller, H. Shemer, and R. Semiat, "Energy and environmental issues in desalination," *Desalination*, vol. 366, pp. 2–8, 2015.

[2] A. Siddiqi and L. D. Anadon, "The water–energy nexus in Middle East and North Africa," *Energy Policy*, vol. 39, no. 8, pp. 4529–4540, 2011.

[3] N. Ghaffour, T. M. Missimer, and G. L. Amy, "Technical review and evaluation of the economics of water desalination: Current and future challenges for better water supply sustainability," *Desalination*, vol. 309, pp. 197–207, Jan. 2013.

[4] S. Lattemann and T. Höpner, "Environmental impact and impact assessment of seawater desalination," *Desalination*, vol. 220, no. 1–3, pp. 1–15, Mar. 2008.

[5] F. Trieb and H. Müller-Steinhagen, "Concentrating solar power for seawater desalination in the Middle East and North Africa," *Desalination*, vol. 220, no. 1–3, pp. 165–183, 2008.

[6] M. Shatat, M. Worall, and S. Riffat, "Opportunities for solar water desalination worldwide: Review," *Sustain. Cities Soc.*, vol. 9, pp. 67–80, 2013.

[7] F. Trieb, H. Müller-Steinhagen, J. Kern, J. Scharfe, M. Kabariti, and A. Al Taher, "Technologies for large scale seawater desalination using concentrated solar radiation," *Desalination*, vol. 235, no. 1–3, pp. 33–43, 2009.

[8] P. Palenzuela, D.-C. Alarcón-Padilla, and G. Zaragoza, "Large-scale solar desalination by combination with CSP: Techno-economic analysis of different options for the Mediterranean Sea and the Arabian Gulf," *Desalination*, vol. 366, pp. 130–138, 2015.

[9] S. Al-Kharabsheh and D. Yogi Goswami, "Analysis of an innovative water desalination system using low-grade solar heat," *Desalination*, vol. 156, no. 1–3, pp. 323–332, Aug. 2003.

[10] M. Abutayeh, D. Yogi Goswami, and E. K. Stefanakos, "Theoretical and Experimental Simulation of Passive Vacuum Solar Flash Desalination," *J. Sol. Energy Eng.*, vol. 135, no. 2, Jan. 2013.

[11] A. E. Muthunayagam, K. Ramamurthi, and J. R. Paden, "Modelling and experiments on vaporization of saline water at low temperatures and reduced pressures," *Appl. Therm. Eng.*, vol. 25, no. 5–6, pp. 941–952, 2005.

[12] A. E. Muthunayagam, K. Ramamurthi, and J. R. Paden, "Low temperature flash vaporization for desalination," *Desalination*, vol. 180, no. 1–3, pp. 25–32, Aug. 2005.

[13] Y. Ikegami, H. Sasaki, T. Gouda, and H. Uehara, "Experimental study on a spray flash desalination (influence of the direction of injection)," *Desalination*, vol. 194, no. 1–3, pp. 81–89, Jun. 2006.

[14] S. Mutair and Y. Ikegami, "Experimental study on flash evaporation from superheated water jets: Influencing factors and formulation of correlation," *Int. J. Heat Mass Transf.*, vol. 52, no. 23–24, pp. 5643–5651, 2009.

[15] M. Witt, "Installation for producing solar thermal energy," *U.S. Pat. US 6,367,257 B1*, 2002.

[16] Y. Zhang, J. Wang, J. Yan, D. Chong, and L. Jiping, "Experimental study on energy transformation and separation characteristic of circulatory flash evaporation," *Int. J. Heat Mass Transf.*, vol. 99, pp. 862–871, 2016.

[17] R. Rizaldy, S. J. Zarrouk, and C. Morris, "Liquid carryover in geothermal steam-water separators," in *Proceedings the 38th New Zealand Geothermal Workshop*, 2016.

[18] S. J. Zarrouk and M. H. Purnanto, "Geothermal steam-water separators: Design overview," *Geothermics*, vol. 53, pp. 236–254, Jan. 2015.

[19] H. Lazalde-Crabtree, “Design Approach of Steam-water Separators and Steam Dryers for Geothermal Applications,” *Geothermal Resour. Counc. Bull.*, vol. 13, no. September, pp. 11–20, 1984.
[20] H. Kürten, J. Raasch, and H. Rumpf, “Beschleunigung eines kugelförmigen Feststoffteilchens im Strömungsfeld konstanter Geschwindigkeit,” *Chemie Ing. Tech. - CIT*, vol. 38, no. 9, pp. 941–948, Sep. 1966.
[21] G. Wedler and H.-J. Freund, *Lehrbuch der Physikalischen Chemie*. Wiley-VCH, 2012.
[22] A. Albrecht, “Experimentelle Untersuchungen zur Entspannungsverdampfung von Wasser an einer Technikumsanlage,” Bachelor Thesis, Karlsruhe Institute of Technology (KIT), 2014.

8 Nomenclature

Latin Letters			**Indices**	
d	diameter	m	exp	experimental
F	force	N	g	gas
H	height	m	l	liquid
m	mass	kg	opliq	operating liquid
$\dot{N}$	molar flow rate	kg/s	sat	saturated
p	pressure	Pa		
t	time	s	**Abbreviations**	
T	temperature	K	MSF	Multi Stage Flash
v	velocity	m/s	WRP	water ring pump
$\dot{V}$	volume flow rate	m³/s		
x	vapor content (mass fraction)	kg/kg		